

ChemComm

Accepted Manuscript



This is an *Accepted Manuscript*, which has been through the Royal Society of Chemistry peer review process and has been accepted for publication.

Accepted Manuscripts are published online shortly after acceptance, before technical editing, formatting and proof reading. Using this free service, authors can make their results available to the community, in citable form, before we publish the edited article. We will replace this *Accepted Manuscript* with the edited and formatted *Advance Article* as soon as it is available.

You can find more information about *Accepted Manuscripts* in the [Information for Authors](#).

Please note that technical editing may introduce minor changes to the text and/or graphics, which may alter content. The journal's standard [Terms & Conditions](#) and the [Ethical guidelines](#) still apply. In no event shall the Royal Society of Chemistry be held responsible for any errors or omissions in this *Accepted Manuscript* or any consequences arising from the use of any information it contains.

COMMUNICATION

In-situ observation of facet-dependent oxidation of graphene on platinum in an environmental TEM

Cite this: DOI: 10.1039/x0xx00000x

Received 00th January 2014,
Accepted 00th January 2014

DOI: 10.1039/x0xx00000x

www.rsc.org/

Wentao Yuan,^{‡a} Ying Jiang,^{‡a} Yong Wang,^{*a} Shyam Kattel,^b Zhengfei Zhang,^a Lien-Yang Chou,^c Chia-Kuang Tsung,^c Xiao Wei,^a Jixue Li,^a Xiaofeng Zhang,^d Guofeng Wang,^{*b} Scott X. Mao^{a,b} and Ze Zhang^a

We performed a direct observation of a crystal facet-dependent oxidation of graphene layers on platinum nanocrystals at atomic resolution in an environmental transmission electron microscope. Combining with density functional theory calculations, our work provides a novel approach for the dynamical exploration of the facet-dependent reactions at the atomic level.

Real-time observation of chemical reactions at the atomic scale, which is indispensable to reveal the reaction mechanism, has been long pursued and many methods, such as in-situ environmental transmission electron microscopy (ETEM) and in-situ scanning tunnel microscopy (STM), have been developed to address this issue in the past decades. With atomic resolution imaging, ETEM and STM are widely used to study the structural evolution during the crystal growth,¹⁻³ phase transition,⁴⁻⁷ and gas molecules adsorption,^{8,9} and in particular, to study the catalytic performances of the surfaces of noble-metal nanocrystals¹⁰⁻¹⁸. It is known that the catalytic activities of nanocrystals are largely dependent on their surface structures,¹⁹⁻²¹ and there is no universal rule between the surface structures and catalytic performances.²²⁻²⁵ Considerable experimental progress has been made by comparing the catalytic performance of the catalysts with different surface structures in separate ex-situ experiments or by in-situ experiments performed only for one particular surface per experiment.^{9,17,26,27} However, it should be noted that the comparison between different experiments cannot guarantee an identical reaction condition and so could mislead the identification of factors that determine the catalytic performance. Therefore, it is desirable to conduct simultaneous and in-situ observations regarding catalytic activities on different surfaces within one experiment, which, up to now, has been quite challenging.

In this letter, graphene-layer encapsulated Pt nanocrystals with different crystal facets were developed as an experimental platform to address this challenge. For simplification, we only focus on three typical facets of Pt nanoparticles, i.e., Pt{100}, Pt{110} and Pt{111}. Our experimental design allows a direct observation of different behaviors of graphene oxidation on different Pt surfaces when oxygen was introduced in an ETEM and thereby provides a method for concurrently examining crystal facet-dependent catalytic

reaction. Complementary to the experimental measurements, we performed the first-principles density functional theory (DFT) calculations to elucidate the reaction mechanism and reaction rate for the graphene oxidation reaction on the distinct Pt surfaces.

The graphene-layers coated Pt nanocrystals were fabricated by electron beam irradiation on Pt nanocrystals with a carbon source, as reported previously.²⁸⁻³⁰ In our experiments, Pt nanocrystals (with an average diameter of 6 nm) in an ethanol solution were first dispersed on a Mo micro-grid and then loaded onto the stage in a TEM heating holder. The sample was heated to 500 °C in the ETEM (H-9500, Hitachi Company) until approximately 1 nm-thick amorphous carbon was formed to surround the Pt nanocrystal (Fig. 1a). Under

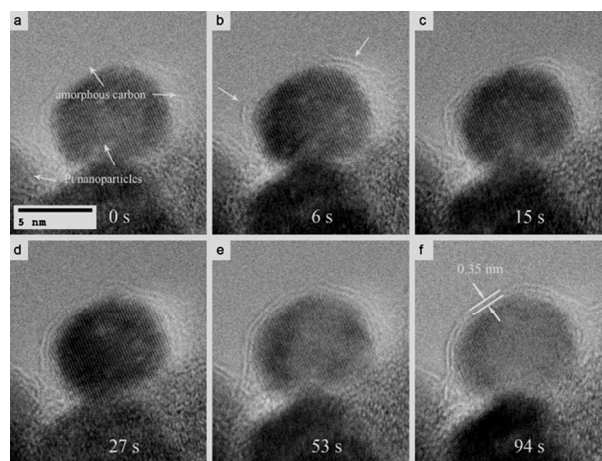


Fig. 1 TEM images showing the in-situ formation process of the graphene layers. (a-f) are series of TEM images from Movie S1, 0 s (a), 6 s (b), 15 s (c), 27 s (d), 53 s (e), 94 s (f). After e-beam irradiation for 6s, partial of the amorphous carbon tends to be in order, marked by arrows in (b). With further irradiation, more regular structures formed and all of the amorphous carbon evolved to graphene layers.

continuous electron beam irradiation for 1~3 minutes, the amorphous carbon was transformed into two carbon layers that are separated by a distance of ~0.35 nm (corresponds to the closest layer distance of graphite), as shown in Fig. 1 (also refer to the supplementary Movie S1 and Fig. S1), suggesting that the fabricated

carbon layers are indeed graphene layers (or one may also call graphite layers).³⁰ In this way, we obtained a reaction system that the graphene layers were directly coated on the multi-faceted Pt nanocrystal surfaces for investigating the graphene oxidation on different Pt nanocrystal surfaces.^{31,32}

Graphene oxidation on the Pt surfaces takes place at 500 °C when oxygen is introduced into the ETEM with a pressure of $\sim 5.00 \times 10^{-2}$ Pa (Movies S2-S5). For visualizing the oxidation of graphene on Pt{100} Pt {110} and Pt{111} facets, we acquired time-lapsed TEM images of the Pt nanocrystals coated by graphene layers in situ during exposure to oxygen environment (Fig. 2 and Movie S2). At the beginning (0s in Fig. 2a, the inset is a colored image of the marked area), the graphene layers fully cover the Pt nanocrystal which protrudes over the substrate. Keeping the oxygen pressure at 5.00×10^{-2} Pa, the graphene layers start to rupture on the edge between {111} and {100} surfaces of the Pt nanocrystal, as shown in Fig. 2b. The initial oxidation on the edges can be ascribed to the low-coordination number (CN) atoms and abundant dangling bonds at the edge sites. These edge sites could greatly facilitate the chemisorptions of the reactant molecules.^{22,33} Also, the low-coordinated sites are considerably different in electronic structure, which makes forming and breaking bonds easier on the edges.^{19,33} We also note that the higher stress arising from the larger curvature at the Pt corners and the stress induced defects may favor to the chemisorptions of the oxygen molecules on the Pt corner and initiate the oxidation of graphene on the edge.

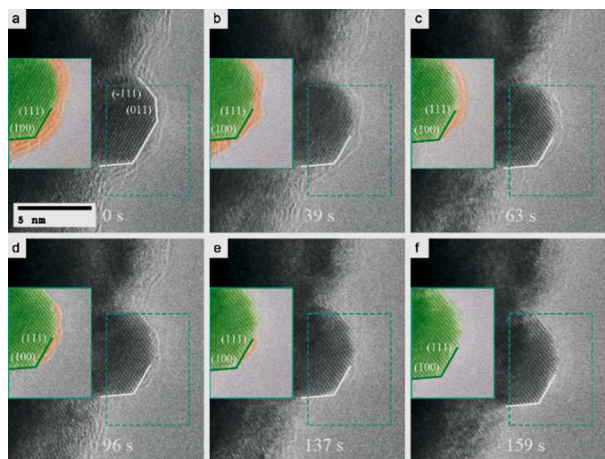


Fig. 2 TEM images of the oxidation of the graphene layers catalyzed by the Pt nanocrystals (sample #1) (at an oxygen pressure of 5.00×10^{-2} Pa, 500 °C), captured at the time of 0 s, 39 s, 63 s, 96 s, 137 s, 159 s, respectively. Here, 0 s corresponds to 86 s in Movie S2. (a) The graphene layers cover the Pt nanocrystal. (b) The graphene layers on the edge between the facets of {111} and {100} first rupture. (c,d) The graphene layers vanish on the surface of {100} facet. (e,f) The graphene layers on the surfaces of {111} facet (e) and other facets (f) disappear in succession. The insets are colored images corresponding to the marked areas in (a-f).

Oxidation of the graphene layers continues on Pt(100) and Pt(111) facets after the rupture on the edge. It should be noted that once the graphene layers rupture on an edge, the stress on the graphene layers will be released, and the rates of subsequent oxidation should solely depend on the catalytic activity of the different surfaces of the Pt nanocrystals. As shown in Figs. 2c-d, graphene oxidation goes on from the right to the left side on Pt(100) surface and from the left to the right side on Pt(111) surface. Based on these in-situ TEM data, the average velocities of graphene oxidation on Pt(100) and Pt(111)

surfaces are estimated to be 0.080 nm/s and 0.025 nm/s, respectively. This result shows that graphene oxidation is much faster on the Pt(100) surface than that on Pt(111) surface, just like what we see on Movie S2. Considering the fact that graphene layers on Pt(100) surface are a little bit thicker than those on Pt(111) facet in Fig. 2b, a higher velocity on Pt(100) surface could be expected. Besides the obvious oxidation difference on Pt(100) and Pt(111) surfaces in Fig. 2, the graphene oxidation on Pt (011) and Pt(-111) surfaces in the same picture should also be considered to acquire a complete picture for the oxidation on different surfaces under the same condition. Based on the in-situ data of Fig.2 (Movie S2), the oxidation rates on (011) and (-111) surfaces are estimated to be 0.053 nm/s and 0.027 nm/s, respectively. This result confirms that the graphene oxidation on the (100) surfaces are faster than that on {111} surfaces and it also shows that Pt(011) surface possesses a faster catalytic oxidation velocity than {111} surfaces. Note that the graphene layers on Pt(011) surface become thinner after those vanished on Pt(-111) (Movie S2). Therefore, the estimated oxidation velocity on Pt(011) surface should be slightly faster than the real situation. Nevertheless, another similar experiment suggests the same result that the oxidation velocity on Pt(110) surface is faster than that on Pt(111) surfaces, as shown in Fig. 3 and Movie S3, where the oxidation rates are estimated to be

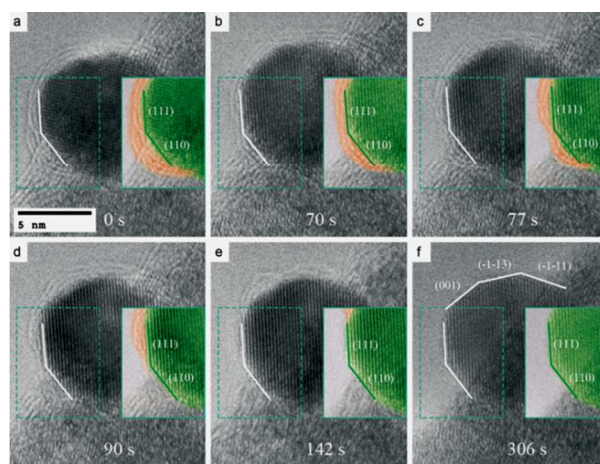


Fig. 3 TEM images of the oxidation of the graphene layers catalyzed by the Pt nanocrystals (sample #2) (at an oxygen pressure of 5.00×10^{-2} Pa, 500 °C), captured at the time of 0 s, 70 s, 77 s, 90 s, 142 s, 306 s, respectively. Here, 0 s corresponds to 18 s in Movie S3. (a) The graphene layers cover the Pt nanocrystal. (b,c) The graphene layers on the edge between the facets of {111} and {110} first rupture. (d) Graphene layers vanish on the surface of {110} facet. (e,f) The graphene layers on the surfaces of {111} facet (e) and other facets (f) disappear in succession. Insets are colored images corresponding to the marked areas in (a-f).

0.183 nm/s and 0.04 nm/s for Pt(110) and Pt(111), respectively. To acquire a statistic result, we have calculated the velocities on thirteen typical facets (i.e., {100}, {110} and {111}) exposed in our four samples, as summarized in Table 1. One can see that almost all of these velocities are consistent with our conclusion that the oxidation of graphene layers are more rapid on Pt{100} and Pt{110} surfaces than that on Pt{111} facets. However, it should be noted that the velocity on Pt(100) facet on Sample #2 (Fig. 3 and Movie S3) is slightly lower than that on Pt(111) facet, which seems in contrast to the conclusion. However, if looking at the image and video carefully (Fig. 3 and Movie S3), one may observe that the graphene layers on Pt (100) facet formed a promontory and lost the close surface contact with Pt (100) facet during the oxidation, which results in a lower

reaction velocity. This result in turn indicates that the facet plays an important role in the oxidation of graphene layers. We also note a (-1-13) facet in Fig. 2, which is seldom observed in our extensive experiments.

Table 1 The line oxidation velocities of the graphene layers on different facets.

	Sample #1 (Fig. 2)	Sample #2 (Fig. 3)	Sample #3 (Fig. S3)	Sample #4 (Fig. S2)
velocity (nm/s)				
(100)	0.080	0.029	0.104	0.070
(110)/(011)	0.053	0.183	0.077	0.077
(111)/(-111)	0.025/0.027	0.040	0.018/0.028	0.033

It is worth noting here that the in-situ observation is based on projected TEM images and the surfaces become lines in the images. Therefore, the area of these surfaces need be considered to acquire a full picture of the oxidation rate on different surfaces. To this end, we established a simplified 3D model only three typical {100}, {110} and {111} surfaces involved to estimate the discrepancies of the oxidation rates (the details are described in the Supplementary Information). For simplicity, only Sample #1 and Sample #3 were considered. Calculations based on this model (Fig. S4) produce a minimum oxidation rate of 0.075 nm²/s and 0.094 nm²/s for {100} facets and {110} facets, respectively; and a maximum oxidation rate of 0.067 nm²/s for {111} facets in sample #1. It is obvious that the maximum oxidation rates on Pt{111} surfaces are less than those minimum rates on Pt(100) and Pt(011) surfaces, which is consistent with the results based on Fig. 2 that the graphene oxidation rates on Pt(100) and Pt(110) surfaces are faster than that on Pt{111} facets. We obtained similar results for Sample #3, as shown in Table S1. However, it is rather difficult to compare the oxidation rates on {100} and {110} surfaces based on this simple model since the calculated results only show their minima. Nevertheless, the 3D model shows the same result that Pt{100} and Pt{110} facets are more active than Pt{111} facets for the oxidation of graphene layers.

In order to understand how oxidation of graphene layers proceeds more rapidly on Pt{100} (or {110}) than that on the facets of Pt{111}, we first rule out other factors involved in the experiments, such as defects in the graphene or defects that could be produced from the electron beam. The impact of the defects in the graphene layers is believed to be insignificant due to the powerful self-healing function of the graphene layers at high temperatures.^{31,32,34} When a carbon atom is removed from its position by E-beam irradiation, the vacancy will vanish soon by a self-rearrangement.^{32,34} Furthermore, comparison experiments confirm that without introducing oxygen, the graphene layers were observed not removed even under the electron beam irradiation for 10 min, which is far longer than the oxidation time of graphene (1-3 min). One can then conclude that the e-beam irradiation damage has non-essential effects on our results. More details concerning effect of the electron beam or background species involved in the reaction were discussed in the Supplementary Information.

In order to explore the mechanisms for the graphene oxidation process on different Pt facets, we carried out density functional theory (DFT) calculations (for details of the computational methods see Supplementary Information) for the catalytic oxidation of graphene to CO₂. Firstly, we calculated the binding energy of chemical species O₂ (reactant), O (intermediate) and CO₂ (product) on Pt{111} (CN=9), Pt{100} (CN=8) and Pt{110}(CN=7) surfaces. Our calculated binding energies for O₂ on Pt{111}, Pt{100} and

Pt{110} surfaces are -0.65eV, -1.10eV, and -1.59eV, whereas for O on these surfaces are -3.96eV, -4.03eV, and -4.23 eV, respectively. Our results show that low coordinated Pt({100} and {110}) surfaces bind O₂ and O more strongly compared to the closely packed Pt {111} surface. This implies that the reactant (O₂) is preferably adsorbed on the low coordinated Pt surfaces for the further oxidation reactions. In contrast, the DFT results show that CO₂ does not chemically bind on any of the Pt surfaces (the binding energies of CO₂ are calculated to be -0.05eV, -0.04eV, and -0.06 eV on {111}, {100} and {110} surfaces, respectively). Therefore, the oxidation reaction product, CO₂, would be more likely to be desorbed than bind to the Pt surface after it is formed. Secondly, we studied the O₂ dissociation reaction (O₂→2O) on closely packed Pt{111} surfaces and low coordinated Pt{100} surfaces. The activation energy for O₂ dissociation on the low coordinated Pt{100} surface is 0.15 eV,³⁵ which is significantly lower than that (0.63 eV) on the closely packed Pt{111} surface.³⁶ Therefore, dissociation of O₂ to 2O is kinetically favorable on Pt{100} surfaces compared to that on Pt{111} surfaces. As a result, reactive O species will thus be readily available for the oxidation of graphene (to CO₂) covering Pt{100} surface when O₂ is introduced into the system. Next, we discuss the possible routes for O₂ to reach the Pt surfaces. Since Pt nanocrystals are covered by graphene layers, there are two possibilities. One is directly reaching the surface at the opening edge and the other is through the defects of the graphene layers. At the beginning stage, since there is no obvious opening in the graphene layers, the oxygen molecules may reach the Pt edges and corners through the defects of graphene layers on the Pt edges. Once an opening formed in the graphene layers, the oxygen molecules pass through the opening and the oxidation goes along the graphene edges. One can expect that if the defects dominate the whole reaction, the graphene layers could disappear everywhere, at least, not just along the opening edges as shown in our experiments. Based on this fact, we could conclude that the oxygen molecules reach the Pt surface through the defects at the beginning of the oxidation and then through the opening area as soon as it is formed.

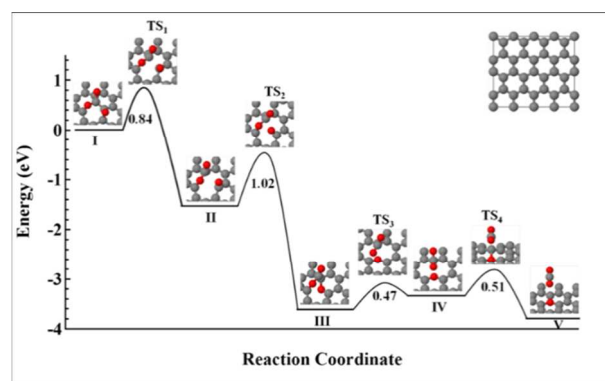


Fig. 4 Mechanism of the C-C bond breaking in graphene and CO₂ formation in the presence of 3O species adsorbed on a defect-free graphene sheet. I, II, III, IV and V represent the various lowest energy configurations of 3O species adsorbed on the graphene. TS1, TS2, TS3 and TS4 represent the transition states for steps: I→II, II→III, III→IV and IV→V, respectively. All the activation energies are given in unit of eV. The plot on the top right corner depicts the graphenesupercell used in our DFT calculations. In the figure, the gray balls represent C atoms, and the red balls represent O atoms.

Finally, we studied the possible mechanism of the C-C bond breaking in a monolayer graphene. Fig. 4 illustrates the mechanism of C-C bond breaking in graphene and the oxidation of graphene to form CO₂ molecules when O species are adsorbed on the pristine graphene surface.³⁷As shown in Fig. 4, formation of CO₂ is

exothermic by about 3.8eV when 3O species are adsorbed on the graphene in the most stable adsorption configuration. In detail, step I-II involves the C-C bond breaking in the graphene which requires activation energy of 0.84 eV. Step II-III involves the formation of a C₅O hexagon in the graphene basal plane with activation energy of 1.02 eV. Step III-IV involves the re-orientation of O-C-O group so that 2O atoms (above the graphene plane) are solely bound to a single C atom that remains protruded out of the graphene plane. This particular step is endothermic by 0.22 eV and has activation energy of 0.47 eV. The final step IV-V involves desorption of CO₂ molecule from the graphene surface. The activation energy for this step is calculated to be 0.51 eV. Here, our DFT calculations show that the breaking of the C-C bond in graphene basal plane and the oxidation of graphene is energetically possible in the presence of atomic O species. Because of kinetically favored O₂ adsorption and dissociation on the low coordinated Pt{100} surfaces over closely packed Pt{111} surfaces, which are essential to initiate graphene oxidation by producing atomic O species, the breaking of the C-C bond and rupturing of graphene surface would be more facilitated on Pt{100} facets than Pt{111} facets. Consequently, the DFT results corroborates the experimental observation that the oxidation of the graphene layers would occur earlier and more rapidly on low coordinated Pt{100} surfaces compared to closely packed Pt{111} surfaces.

In conclusion, we have presented the first example of an in-situ observation of facet-dependent reaction on nanocrystal-catalyst surfaces. The oxidation processes of graphene layers on different facets of Pt nanocrystals were monitored by an ETEM. It is found that the graphene oxidation occurs preferentially on Pt{100} and Pt{110} facets compared to Pt{111} facets. The DFT calculation reveals that such facet-dependent catalytic reaction is a result of the higher reactivity of {100} (or {110}) surfaces towards the adsorption of reaction species and the dissociation of O₂ to atomic O species than that of Pt{111} surfaces. Our work provides a direct experimental evidence of facet-dependent reaction at the atomic scale and offers a new platform to investigate the mechanism of catalytic reactions for other nanocrystal systems.

We acknowledge the support of National Science Foundation of China (51390474, 11234011), Program for Innovative Research Team in University of Ministry of Education of China (IRT13037), Key Science and Technology Innovation Team of Zhejiang Province (2010R50013) and National Young 1000 Talents Program of China.

Notes and references

*These authors contributed equally.

^aCenter of Electron Microscopy and State Key Laboratory of Silicon Materials, Department of Materials Science and Engineering, Zhejiang University, Hangzhou 310027, China.

E-mail: yongwang@zju.edu.cn

^bDepartment of Mechanical Engineering and Materials Science, University of Pittsburgh, Pittsburgh, PA 15261, USA.

E-mail: guw8@pitt.edu

^cDepartment of Chemistry, Boston College, Chestnut Hill, MA 02467.

^dHitachi High Technologies America, Pleasanton, CA 94588, USA.

† Electronic supplementary information (ESI) available: Experimental details, supplementary figures and movies. See DOI: 10.1039/c000000x/

1 F. M. Ross, *Reports on Progress In Physics* **2010**, *73*;

- 2 H. M. Zheng, R. K. Smith, Y. W. Jun, C. Kisielowski, U. Dahmen, A. P. Alivisatos, *Science* **2009**, *324*, 1309-1312;
- 3 S. Helveg, C. Lopez-Cartes, J. Sehested, P. L. Hansen, B. S. Clausen, J. R. Rostrup-Nielsen, F. Abild-Pedersen, J. K. Nørskov, *Nature* **2004**, *427*, 426-429.
- 4 F. Tao, M. Salmeron, *Science* **2011**, *331*, 171-174;
- 5 H. M. Zheng, J. B. Rivest, T. A. Miller, B. Sadtler, A. Lindenberg, M. F. Toney, L. W. Wang, C. Kisielowski, A. P. Alivisatos, *Science* **2011**, *333*, 206-209;
- 6 S. Takeda, H. Yoshida, *J. Electron Microsc.* **2013**, *62*, 193-203;
- 7 J. R. Jinschek, *Chemical Communications* **2014**, *50*, 2696-2706.
- 8 H. Yoshida, Y. Kuwauchi, J. R. Jinschek, K. Sun, S. Tanaka, M. Kohyama, S. Shimada, M. Haruta, S. Takeda, *Science* **2012**, *335*, 317-319;
- 9 Y. Wang, H. J. Sun, S. J. Tan, H. Feng, Z. W. Cheng, J. Zhao, A. D. Zhao, B. Wang, Y. Luo, J. L. Yang, J. G. Hou, *Nature Communications* **2013**, *4*.
- 10 P. L. Hansen, J. B. Wagner, S. Helveg, J. R. Rostrup-Nielsen, B. S. Clausen, H. Topsøe, *Science* **2002**, *295*, 2053-2055;
- 11 P. L. Gai, E. D. Boyes, S. Helveg, P. L. Hansen, S. Giorgio, C. R. Henry, *Mrs Bulletin* **2007**, *32*, 1044-1050;
- 12 K. Kishita, H. Sakai, H. Tanaka, H. Saka, K. Kuroda, M. Sakamoto, A. Watabe, T. Kamino, *J. Electron Microsc.* **2009**, *58*, 331-339;
- 13 T. Uchiyama, H. Yoshida, Y. Kuwauchi, S. Ichikawa, S. Shimada, M. Haruta, S. Takeda, *Angewandte Chemie-International Edition* **2011**, *50*, 10157-10160;
- 14 Y. Kuwauchi, H. Yoshida, T. Akita, M. Haruta, S. Takeda, *Angewandte Chemie-International Edition* **2012**, *51*, 7729-7733;
- 15 T. Yaguchi, T. Kanemura, T. Shimizu, D. Imamura, A. Watabe, T. Kamino, *J. Electron Microsc.* **2012**, *61*, 199-206;
- 16 J. C. Yang, M. W. Small, R. V. Grieshaber, R. G. Nuzzo, *Chemical Society Reviews* **2012**, *41*, 8179-8194;
- 17 J. Inukai, D. A. Tryk, T. Abe, M. Wakisaka, H. Uchida, M. Watanabe, *Journal Of the American Chemical Society* **2013**, *135*, 1476-1490;
- 18 H. L. L. Xin, S. Alayoglu, R. Z. Tao, A. Genc, C. M. Wang, L. Kovarik, E. A. Stach, L. W. Wang, M. Salmeron, G. A. Somorjai, H. M. Zheng, *Nano Letters* **2014**, *14*, 3203-3207.
- 19 G. A. Somorjai, D. W. Blakely, *Nature* **1975**, *258*, 580-583;
- 20 R. R. Adzic, A. V. Tripkovic, W. E. Ogrady, *Nature* **1982**, *296*, 137-138;
- 21 G. Ertl, *Angewandte Chemie-International Edition* **2008**, *47*, 3524-3535.
- 22 G. A. Somorjai, F. Zaera, *Journal of Physical Chemistry* **1982**, *86*, 3070-3078;
- 23 S. G. Sun, A. C. Chen, T. S. Huang, J. B. Li, Z. W. Tian, *Journal Of Electroanalytical Chemistry* **1992**, *340*, 213-226;
- 24 J. Perez, H. M. Villullas, E. R. Gonzalez, *Journal of Electroanalytical Chemistry* **1997**, *435*, 179-187;
- 25 A. V. Tripkovic, K. D. J. Popovic, J. D. Lovic, *J. Serb. Chem. Soc.* **2003**, *68*, 849-857.
- 26 R. Narayanan, M. A. El-Sayed, *Nano Letters* **2004**, *4*, 1343-1348;
- 27 K. M. Bratlie, H. Lee, K. Komvopoulos, P. Yang, G. A. Somorjai, *Nano Letters* **2007**, *7*, 3097-3101.
- 28 F. Banhart, *Reports on Progress In Physics* **1999**, *62*, 1181-1221;
- 29 X. Ge, B. H. Peng, X. B. Ying, R. Wang, X. Y. Liu, F. S. Xiao, S. L. Qiu, J. X. Li, *Carbon* **2008**, *46*, 1411-1416;
- 30 Z. Peng, F. Somodi, S. Helveg, C. Kisielowski, P. Specht, A. T. Bell, *Journal of Catalysis* **2012**, *286*, 22-29.
- 31 T. Fuller, F. Banhart, *Chemical Physics Letters* **1996**, *254*, 372-378;
- 32 F. Banhart, *J. Electron Microsc.* **2002**, *51*, S189-S194.
- 33 G. A. Somorjai, *Science* **1985**, *227*, 902-908.
- 34 J. Chen, T. Shi, T. Cai, T. Xu, L. Sun, X. Wu, D. Yu, *Applied Physics Letters* **2013**, *102*, 103107.
- 35 Z. Duan, G. Wang, *J. Phys. Chem. C* **2013**, *117*, 6284-6292.
- 36 Z. Duan, G. Wang, *Physical Chemistry Chemical Physics* **2011**, *13*, 20178-20187.
- 37 R. Larciprete, S. Fabris, T. Sun, P. Lacovig, A. Baraldi, S. Lizzit, *Journal of the American Chemical Society* **2011**, *133*, 17315-17321.